

Tidal Energy Extraction in an Idealized Ocean-Fjord Tidal Model with Astronomical Forcing

Mitsuhiro Kawase¹, Marisa Gedney²

*Northwest National Marine Renewable Energy Center
School of Oceanography, University of Washington
Seattle, Washington, 98195 United States*

¹kawase@u.washington.edu

²mgedney@u.washington.edu

Abstract— A highly idealized model of an ocean-fjord system, in which the tide is forced astronomically by the gravitational force of the moon, is used to study effects of localized tidal energy extraction on regional and global tides. The modeled system is energetically complete in the sense that the model does not have an open boundary and the integrated energy balance has no exchange term with the outside ocean. Both normal and tidally near-resonant fjords are considered. A series of energy extraction experiments is performed to establish the scaling between energy extraction and changes in the tidal parameters with in the estuary and the surrounding ocean. These experiments confirm previous theoretical results on the scaling. At maximum extraction, approximately half the energy extracted is redirected from natural dissipation within the fjord, while the remainder is drawn anew from the ocean. The experiments are then repeated with a pair of subdomain models of different domain extent, for which tides sampled from the complete model are used as boundary conditions. The scaling relationship between extraction and tidal parameters in the subdomain models agrees with that of the full-domain model, but the estimate of the maximum extractable energy differ by up to 27%.

Keywords— Tidal energetics, hydrodynamic modeling, resource assessment, environmental impact assessment.

I. INTRODUCTION

Hydrodynamic models of coastal seas and estuaries are now routinely implemented and run for many coastal regions and estuaries around the world. They are starting to see use in resource assessment of tidal energy projects (e.g. [1]–[3]); in future, such models will also be used in appraisals of potential environmental impacts of tidal energy developments. Each such model covers a limited geographical area; the outer boundary of the model includes open segments interfacing the rest of the ocean, where tides are generated by imposed boundary conditions. Direct local forcing of tides is not typically included in these models.

In reality, the tide is an astronomical phenomenon generated by differential gravity of the moon and the sun at the global scale [4]. The tide gains energy at the largest terrestrial spatial scale, and redistributes it around the globe and into the coastal ocean via long waves. Forcing and the response are not separable, and are expected to interplay at the global scale. This raises a question of well-posed-ness of limited-domain hydrodynamic models as a mathematical problem when they are applied to problems in which tides are actively modified within the model domain, such as

simulations of tidal energy extraction ([5], [6]). The level of uncertainty in the conclusions that can be drawn from the results of these numerical models is as yet unclear, even though the knowledge of this uncertainty will be critically important to investors in and insurers of tidal energy installations. No previous study has addressed tidal energy extraction in the context of a complete energy balance.

Rather than pursuing the question of appropriate boundary conditions further, we have decided to model an idealized system that has the tide forced the way it is in reality, namely, by tide-generating force from a heavenly body. The model consists of a simple square ocean basin where the tide is generated; and an embayment in the shape of a simple sill fjord, where a strong tidal current results and energy extraction is attempted. The main reason for pursuing such a model is to study energetic balance of tidal power generation with both supply and loss properly accounted for. Initial theoretical work on extractable power from tidal currents has generally regarded the existence of a strong current resource as a given (e.g. [7], [8]); however, since mechanical energy between forcing and dissipation is a conserved quantity, we believe the answer to the problem of resource assessment must include physical understanding of how the energy is supplied to the system.

Such a system can be simulated with modest computational resource, since ocean tide has large spatial scale (of the same order as the size of the ocean basin) and can be well resolved with a relatively coarse grid. Use of a variable-mesh grid with a coarser resolution over the ocean and a refined resolution in and around the fjord is a key element of such a model. It must also be assumed that detailed tidal processes in the ocean part that cannot be resolved, such as tidal dissipation in a specific locale, will not critically affect the physics of tidal energy extraction in the fjord. This appears to be a reasonable assumption, but admittedly it is an untested one.

Once such a model is set up and studied, it can be used as a benchmark against which to test the behavior of limited-domain models. Namely, the results of the full-domain model will be regarded as “the truth”, and also used to supply boundary conditions to a model that covers only part of the system domain. Energy extraction experiments can be performed in the subdomain model, and their results can be compared with those using the full-domain model. This way,

at least an empirical sense of uncertainties in the subdomain model results can be obtained.

The set-up of both the full-domain and the subdomain models are described in the section II, and the results presented in the section III. Main findings, their implications and topics for further research are discussed in the section IV.

II. METHODS

The model dynamics and the domain geometry / bathymetry are common to both the full-domain and the subdomain models; they differ only in the domain coverage, as well as that the latter is forced by boundary conditions taken from the former.

Model Equations

The model simulates the tidal response of a single-layer ocean using nonlinear shallow-water equations (Equations 1 – 3) in an equatorial beta-plane coordinate system [9]:

$$u_t + uu_x + vv_y = \beta yv - g\eta_x - \frac{C_N + C_E}{H + \eta} |\bar{u}| u - \phi_x \quad (1)$$

$$v_t + uv_x + vv_y = -\beta yu - g\eta_y - \frac{C_N + C_E}{H + \eta} |\bar{u}| v - \phi_y \quad (2)$$

$$\eta_t + [(H + \eta)u]_x + [(H + \eta)v]_y = 0 \quad (3)$$

Here, (x, y) are the eastward and the northward coordinates, t is time, and subscripts denote partial differentiation. $\bar{u} = (u, v)$ is the horizontal velocity with eastward and northward components respectively; η is sea surface height. β is the gradient of the Coriolis parameter at the equator ($2.29 \times 10^{-11} \text{ m}^{-1} \text{ s}^{-1}$); and g is gravitational acceleration (9.806 m s^{-2}). H is the depth of the undisturbed ocean (a function of x and y).

Tidal forcing is provided by a tidal potential ϕ . Dissipation is represented by quadratic drag. It consists of a natural background (C_N) and local enhancement representing tidal energy extraction (C_E). The former is set at 0.003; the latter is varied to simulate different levels of energy extraction.

These equations are implemented using the barotropic component of the Regional Ocean Modeling System (ROMS) code [10], with modifications for tidal potential and localized energy extraction.

Model Domain

The ocean is an 8000km-wide square basin that straddles the equator symmetrically (Fig.1). The size of this basin is roughly intermediate between the Pacific and the Atlantic Oceans. A continental shelf with a depth of 200m and a width of 500km encircles a deep basin 4000m deep. A 10km-wide fjord-like embayment, with a 50m sill at a 4km-wide constriction, is appended at the northeastern corner (Fig.2). The length of the fjord is set at either 200km, similar to Puget Sound, US; or 400km, making the fjord quarter-wave resonant to the semi-diurnal tide.

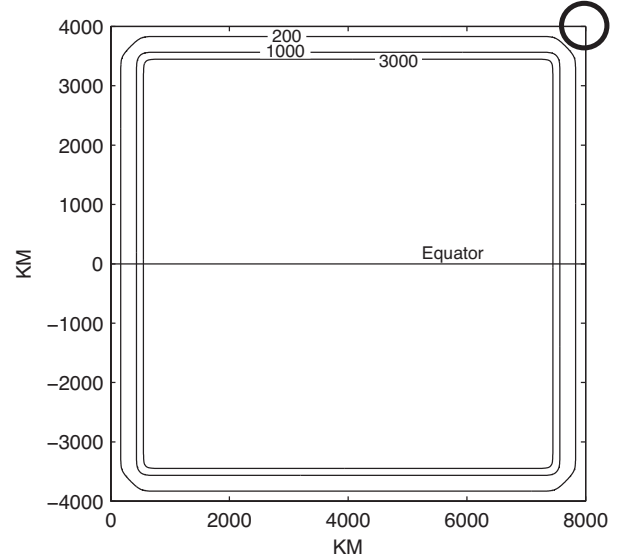


Fig. 1. The model ocean basin showing bathymetric contours in meters. Dark circle indicates the corner on which the fjord is attached.

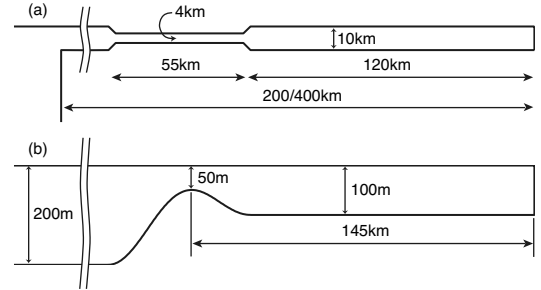


Fig. 2. Geometry of the attached fjord: (a) plane view showing horizontal dimensions and (b) sectional view showing the bathymetry. Ocean is to the left.

Enhanced dissipation C_E is implemented over a 2km-long segment of the fjord centered at the sill. Enhancement covers the entire width of the channel, and the value of C_E is uniform throughout the segment.

The domain is discretized into a stretched structured grid, with a resolution of 500m in the fjord and over the continental shelf in the offshore direction, and up to 20km in the ocean basin.

Forcing

The tidal potential ϕ used here takes an analytical form shown in Equation (4), which approximates the projection of the potential due to a single heavenly body onto the equatorial beta-plane coordinates (see also Fig.3):

$$\phi(x, y, t) = -\phi_0 \left[\cos \theta \cos \left(\frac{x}{R_E} + \Omega t \right) + \sin \theta \frac{y}{R_E} \right]^2 + \phi_0 \sin^2 \theta \frac{y^2}{R_E^2} \quad (4)$$

Here θ is the celestial declination of the heavenly body, R_E is the radius of the earth, and Ω is the angular rotation rate of the earth relative to the body ($2\pi/\Omega$ is the fundamental tidal period). The strength of the potential ϕ_0 is set equal to that of the moon ($3.5119 \text{ m}^2\text{s}^{-2}$); however, for analytical simplicity, the period is set to be exactly twenty-four hours. Thus the tidal response should consist of a single semi-diurnal constituent with a period of twelve hours, a single diurnal constituent with a period of twenty-four hours, and their harmonics. θ is set at 20° from the celestial equator and is fixed. There is no fortnightly or longer timescale variation of the tide.

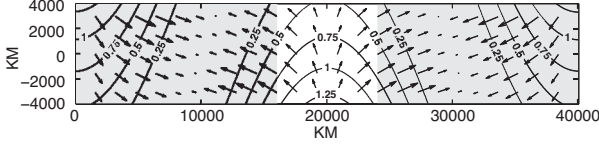


Fig. 3. Tidal potential ϕ (contour, in units of ϕ_0 , c.i.=0.25) and associated tidal acceleration (vectors). The pattern propagates westward (to the left) at the speed ΩR_E . Unshaded area indicates the size of the model domain.

Energy Balance

In the absence of forcing and friction ($\phi = C_N = C_E = 0$), a system described by Equations (1) – (3) conserves total mechanical energy (TME), defined as a domain-wide integral of total mechanical energy density (TMED):

$$\text{TMED} = \frac{1}{2} \rho (H + \eta) |\bar{u}|^2 + \frac{1}{2} \rho g \eta^2$$

where ρ is the density of sea water set at $1,025 \text{ kg/m}^3$. The two terms represent local density of kinetic energy and of potential energy, respectively.

With forcing and friction present, a local energy balance equation can be written as follows:

$$\frac{\partial}{\partial t} \text{TMED} = -\bar{\nabla} \cdot \bar{F} - \rho C_N |\bar{u}|^3 - \rho C_E |\bar{u}|^3 - \rho (H + \eta) \bar{u} \cdot \bar{\nabla} \phi \quad (5)$$

where \bar{F} is horizontal mechanical energy flux:

$$\bar{F} = \frac{1}{2} \rho (H + \eta) |\bar{u}|^2 \bar{u} + \rho (H + \eta) \eta \bar{u}$$

The terms on the right hand side of Equation (5) represent, respectively, convergence of mechanical energy flux; natural dissipation; tidal energy extraction (which in this case includes loss to wake generation, power train inefficiency, and other causes as well as energy gainfully converted to electrical power); and tidal energy gain from forcing.

Once the tide reaches an equilibrium, the average of the left hand side of Equation (5) over a tidal period becomes zero; and a tidal average energy balance equation can be written as

$$\rho C_N \overline{|\bar{u}|^3} + \rho C_E \overline{|\bar{u}|^3} = -\bar{\nabla} \cdot \bar{F} - \rho \overline{(H + \eta) \bar{u} \cdot \bar{\nabla} \phi} \quad (6)$$

Here, the overbar denotes tidal averaging:

$$\overline{(*)} = \frac{\Omega}{2\pi} \int_t^{t+2\pi/\Omega} (*) dt$$

Equation (6) can also be cast in an integral form over any subdomain Γ of the model:

$$\begin{aligned} \iint_{\Gamma} \rho C_N \overline{|\bar{u}|^3} dA + \iint_{\Gamma} \rho C_E \overline{|\bar{u}|^3} dA \\ = - \int_{\partial\Gamma} \bar{n} \cdot \bar{F} dl - \iint_{\Gamma} \rho \overline{(H + \eta) \bar{u} \cdot \bar{\nabla} \phi} dA \end{aligned} \quad (7)$$

The line integral on the right hand side of Equation (7) is to be evaluated over all open segments of the subdomain boundary, and represents influx of mechanical energy across the boundary.

All terms in Equations (6) and (7) can be readily calculated in a numerical model, and are used as diagnostics of the model results.

Subdomain Models

As mentioned in Introduction, practically all models used for tidal energy-related studies have been limited-domain models. One of the goals of this study is to explore the consequences of limited domain representation, and especially to quantify uncertainty it may introduce into quantitative conclusions drawn from results of such a model. Accordingly, models that each covers only a part of the domain shown in Fig. 1 (henceforth called the “full domain”) have been implemented. Each subdomain model includes the fjord, and differs only in the extent of the adjacent ocean covered (Fig.4).

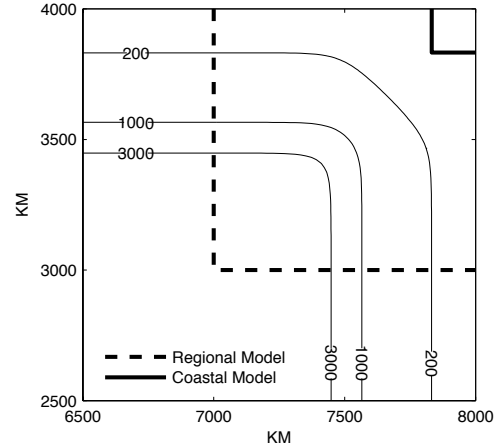


Fig. 4. North-eastern corner of the model domain showing the boundaries of the Regional (dashed line) and the Coastal (solid line) models. Depth contours in meters are also shown.

The “Regional” model covers the north-eastern corner of the full domain including deep waters off the continental shelf.

The ‘‘Coastal’’ model covers only the continental shelf waters adjacent to the fjord. A third subdomain model, which contains the fjord part of the domain only and which takes its boundary conditions at the mouth of the fjord, was implemented but was found to give results greatly at variance with the behaviour of the full-domain model. It was not pursued further and will not be reported here.

Both the Regional and the Coastal models inherit the bathymetry and the grid of the full-domain model. Tidal boundary conditions are taken from the output of the full-domain model, and applied along the open boundary as Dirichlet boundary conditions. Tidal potential ϕ can be switched on or off in the subdomain models. Direct local forcing of tides is not routinely implemented in coastal models; effects of incorporating this are explored in some of the experiments.

III. RESULTS

For all experiments, the model was run for sixty days to bring up the tide to an equilibrium; then for another ten days for sampling and analysis. Select cases were run for further one-hundred days to ensure that stable statistics and energy integrals are obtained.

A. Tides in the Full-domain Model

Tidal response of the oceanic portion of the model is summarized in terms of co-tidal charts (see [4]) in Fig.5. The semi-diurnal tide is progressive with several amphidromic points seen in the basin, notably at the corners of the deep basin (Fig.5 left). Amplitude of the semi-diurnal tide is highest in the corner regions of the domain including at the mouth of the fjord, where it reaches 0.5m. The diurnal tide, on the other hand, takes the form of a basin-wide standing oscillation between the northern and the southern hemispheres (Fig 5 right). Its amplitude is highest in the north-western and the south-western corners, where it reaches 0.17m.

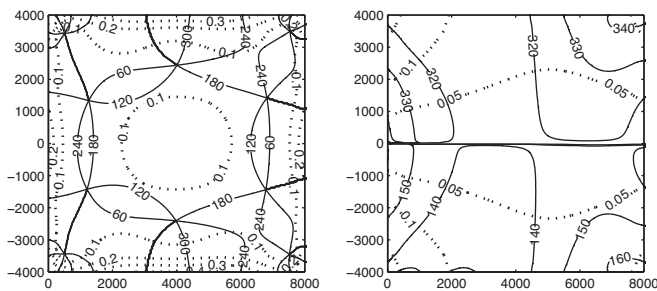


Fig. 5. Semi-diurnal (left) and diurnal (right) co-tidal charts for the model ocean basin (non-resonant case). Amplitude (dotted) is in meters and phase (solid) is in degrees.

The tide in the fjord is dominantly semi-diurnal in both the non-resonant and the resonant cases (Fig. 6). The tidal range in the resonant case is twice as large as the non-resonant case throughout the fjord interior (Fig.7a). The maximum current occurs over the sill, where it reaches 1.3 m/s and 2.5 m/s for the non-resonant and the resonant cases, respectively (Fig. 7b). Subsidiary maxima in the current amplitude to the left and the

right of the sill correspond to exit jets from the sill constriction.

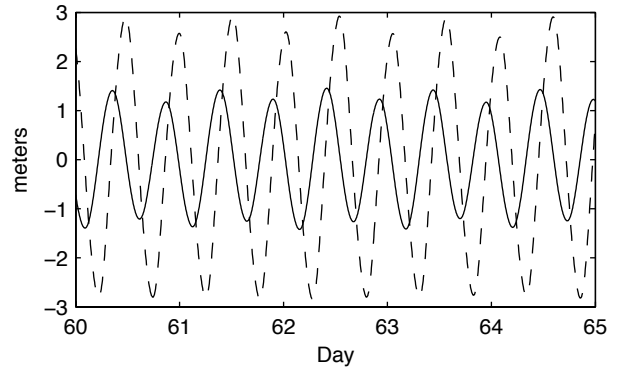


Fig. 6. Sea-surface height at the head of the fjord over a five-day period for the non-resonant (solid line) and the resonant (dashed) cases.

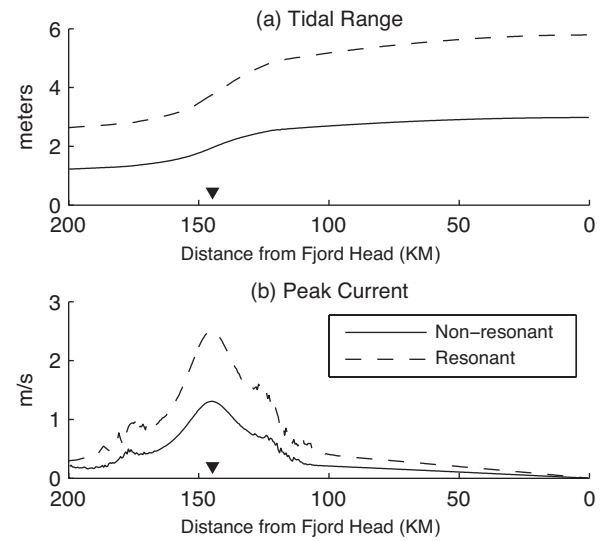


Fig. 7. (a) Tidal range and (b) Peak tidal current in the fjord as a function of distance from the head (to the right in the plots). Solid line indicates the non-resonant case; dashed line indicates the resonant case. Small triangle indicates the location of the sill.

In the non-resonant case, the entire system gains and dissipates mechanical energy at a rate of 1,066 megawatts (MW). This is a very low level of dissipation compared with the estimate for the global ocean [11], and is so low due to the smoothness of the bathymetry (to ensure it is well resolved with a moderate-size grid) and the low level of background bottom friction. Of this, 181MW is being dissipated in the fjord, mainly over the sill region. In the resonant case, the total dissipation is 2,496MW, of which 1,492MW is dissipated in the fjord. In the resonant case, the fjord is the main site of tidal energy dissipation in the entire system.

B. Energy Extraction in the Full-domain Model

The extraction peaks at 247MW and 657MW for the non-resonant and the resonant cases respectively (Fig. 8a), with a corresponding reduction in tidal prism of 34% and 37% (Fig.

8b). An analytical formula for peak extraction from the theoretical study that best approximates this model set-up, that of Blanchfield et al. [12], gives estimates for peak extraction of 274~371MW for the non-resonant case and 522~707MW for the resonant case with parameters from this model. The model result is somewhat low compared with this in the non-resonant case, but is in good agreement for the resonant case. The maximum is reached with a smaller value of the drag coefficient in the resonant case than otherwise (0.05 vs. 0.15). This may be due to the nonlinear nature of the drag: because energy extraction is proportional to the cube of the current speed, the maximum in energy extraction may be reached with a smaller coefficient with higher natural current velocity, if other factors are comparable.

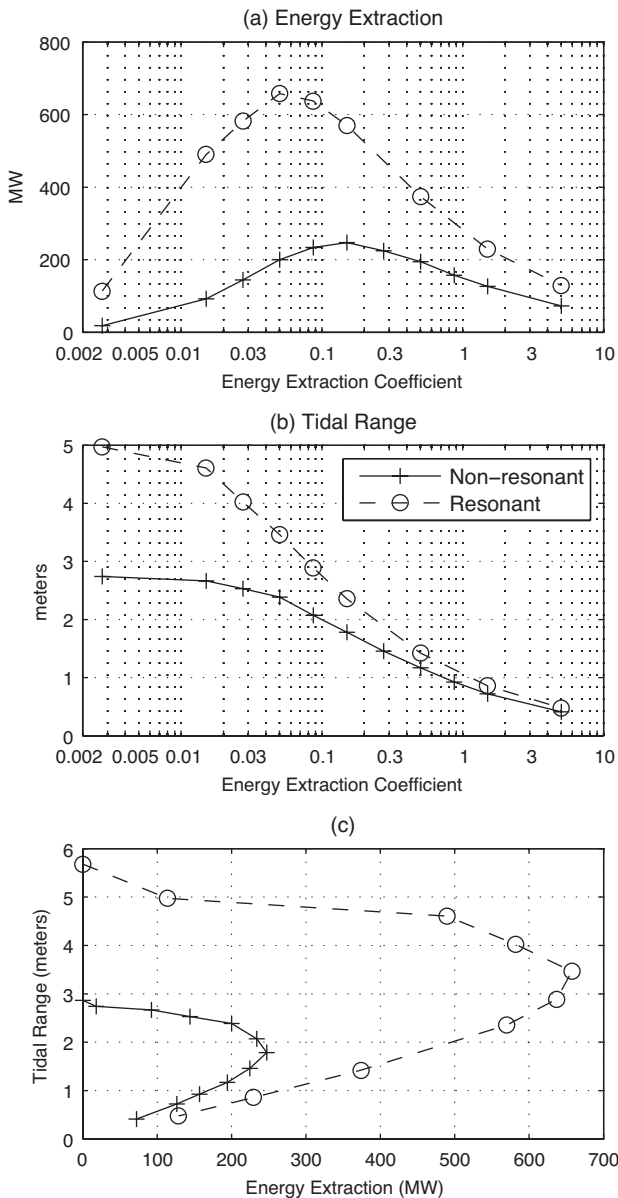


Fig. 8. (a) Energy extraction as a function of extraction drag coefficient C_E . (b) Tidal range at the head of the fjord as a function of C_E . (c) Energy extraction versus tidal range (including the no-extraction case).

In both the non-resonant and the resonant cases, there is an initial, relatively steep drop in tidal range as energy is extracted (Fig. 8c); this drop is relatively larger for the resonant case than the non-resonant case. Beyond this, there is a range over which the same amount of energy extraction results in relatively less reduction in the tidal range. The range becomes again sensitive to extraction as the maximum is approached; beyond this, further increase in C_E results in less extraction because of reduced tidal current and energy loss to long wave reflection, in agreement with theoretical and channel-model studies of energy extraction from oscillatory tidal current ([12], [13]).

Energy extraction results in decreased tidal range throughout the fjord, especially from the sill region inwards (Fig. 9). There is a small drop in tidal range across the energy extraction array, indicating the pressure head that drives the energy extraction. There is also a slight (5 centimetres) increase in the tidal range near the mouth of the fjord in the resonant case.

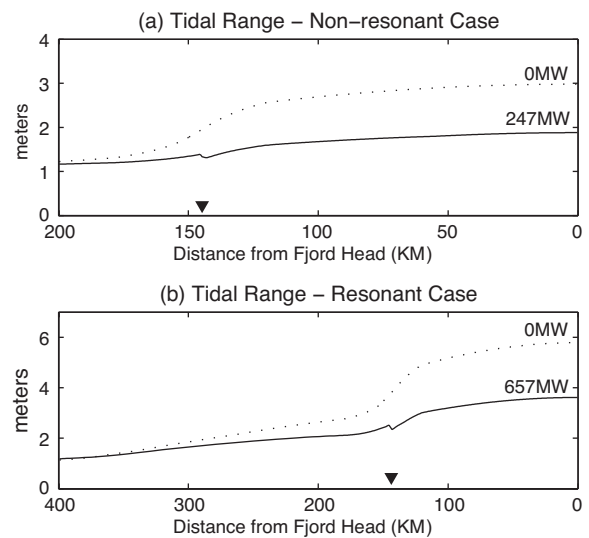


Fig. 9. Tidal range in the fjord for no-extraction (dotted line) and maximum extraction (solid line) cases. (a) Non-resonant case. (b) Resonant case. Triangle denotes the location of the sill / energy extraction.

Some range change is also seen in the ocean outside the fjord (Fig. 10). In the non-resonant case, a small increase is seen to the south-west of the fjord mouth. In the non-resonant case, a somewhat larger increase is seen to the west of the mouth, and a decrease is seen to the south.

One may inquire as to where the source of the extracted energy is in the model domain. Plot of mechanical energy flux in the fjord (Fig. 11a) indicates that the fjord is drawing more mechanical energy from the ocean than in a natural state when energy is extracted. This additional flux (116MW in the maximum extraction case for the non-resonant fjord), however, is much less than the amount of extracted power (247MW). The plot further indicates that, in a natural state, mechanical energy entering the fjord is gradually dissipated over the sill region. When energy extraction is taking place, there is less dissipation of energy until the extraction array is encountered;

there then is an abrupt and large decrease in the mechanical energy flux. Less energy passes the sill crest.

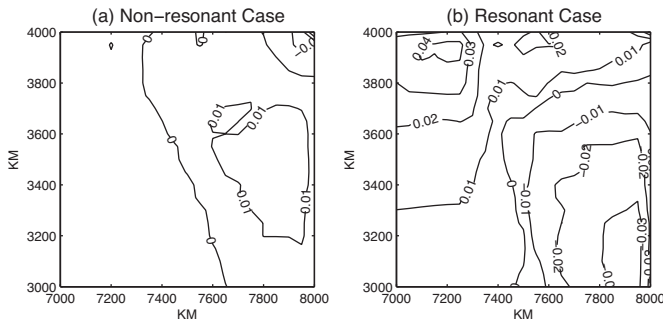


Fig. 10. Change in the tidal range (meters) in the northeast corner of the ocean for maximum energy extraction. (a) Non-resonant case. (b) Resonant case. The fjord mouth is on the upper right corner.

This can be understood by looking at the dissipation due to the natural background friction C_N (Fig. 11b). Because energy extraction reduces tidal prism and the tidal current, natural energy dissipation over the sill region is reduced. At the maximum extraction, most of the energy entering the fjord is extracted by the array. 53% of this is redirected energy from natural dissipation in the fjord, mainly over the sill region.

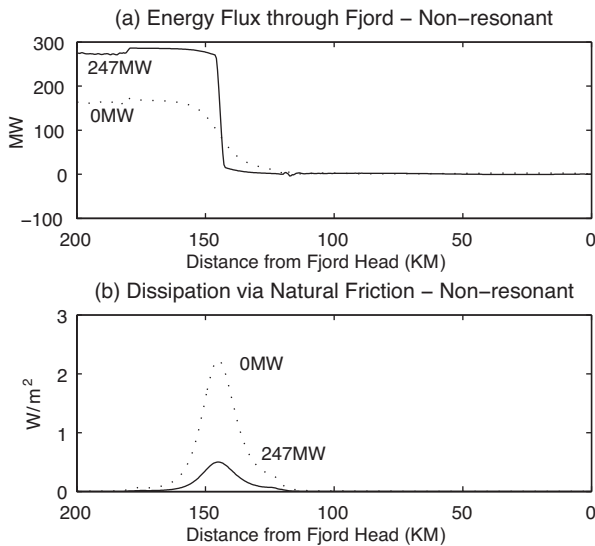


Fig. 11. (a) Cross-channel integrated energy flux in the fjord (MW) for the cases with no extraction (dotted line) and maximum extraction (solid line). (b) Energy dissipation via natural friction (W/m^2) in the fjord. Both plots are for the non-resonant case.

The remaining 47% of energy is drawn from the ocean. This is sourced from the entire ocean basin. One can calculate energy flux coming from beyond certain distance from the fjord mouth. Change in this flux when energy is extracted (Fig. 12) may be considered a measure of the extracted energy coming from a certain distance beyond the fjord mouth. This flux increases slightly with distance initially, then decreases and becomes zero at approximately 1800km away from mouth

of the fjord. However, the sign of the flux then reverses and it becomes greatly negative (away from the fjord). Changes in tidal energy flux due to extraction in the ocean basin (Fig. 13) show a complex pattern throughout the ocean, indicating no discernible outer limit to the source region for the extracted energy, save the entire ocean boundary. Thus, one cannot simply conclude that the extracted energy is coming from within 1800km of the fjord mouth. Evidently, energy extraction in the fjord has a minute but global effect on the tides,

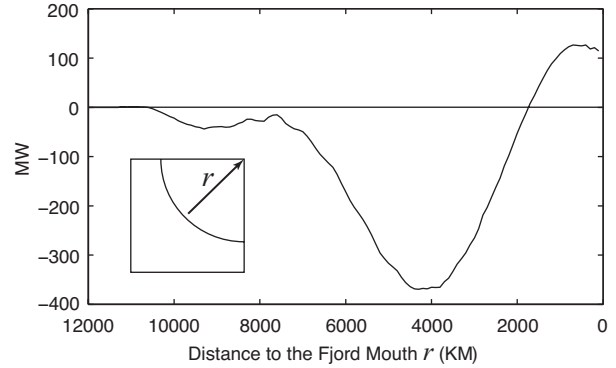


Fig. 12. Difference in energy flux coming from region beyond distance r from the mouth of the fjord between the maximum extraction and the no extraction cases, non-resonant fjord.

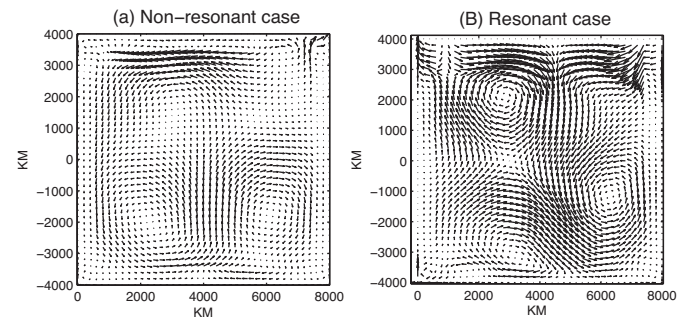


Fig. 13. Difference in the energy flux vector in the ocean basin between the maximum extraction and the no extraction cases. (a) Non-resonant case. (b) Resonant case.

C. Tides in the Subdomain Models and Energy Extraction

The ocean-fjord model and results of energy extraction experiments are now used as benchmarks against which the performance of models whose domain is limited to local waters and whose tide is generated by boundary conditions rather than astronomical forcing.

1) *Tidal Prediction in the Subdomain Models:* The subdomain models were validated by comparing amplitude and phase of the semi-diurnal and the diurnal constituents in the fjord to those from the full-domain model. Interestingly, of the two subdomain models it was the larger of the two, or the “Regional” model, whose tides deviated more from those in the full-domain model. In the non-resonant case, the semi-diurnal amplitude was on average 9.5% deficient compared with the full-domain model (0.45 ~ 1.22m vs. 0.51 ~ 1.34m);

and its phase lagged that in the full-domain model by 15° . Similarly, the diurnal tide was on average 7.4% deficient and was ahead in phase by 6.4° . These are noticeable differences (Fig.14): the RMS error in sea surface height variation at the head of the fjord is 0.26m, which is 8.5% of the tidal range (3m). In the resonant case, the semi-diurnal amplitude was 10.8% too small and the tide lagged in phase by 15.6° ; for the diurnal tide, 8.3% and -8.7° (negative value indicating phase ahead), respectively.

The Coastal model performed better. In the non-resonant case, the semi-diurnal tide amplitude / phase discrepancy was 4.5% / -0.5° and the diurnal tide, 0.1% / -0.2° ; in the resonant case, 3% / -0.05° and 0.7% / -0.5° respectively. In a real-world situation, this level of discrepancy might be difficult to detect when compared with validation data that contain multiple tidal constituents and non-tidal variability.

One reason for the larger discrepancy in the Regional model may be that the boundary of the model lies close to one of the semi-diurnal amphidromic points in the ocean basin. Another may be the absence of direct tidal forcing, which may have a larger effect on a larger-domain model. The latter possibility will be looked at in Section C3 below. No “tuning” or other adjustment was made to the subdomain models; the physics of the subdomain models is kept intentionally as close as possible to the control, which is the full-domain model.

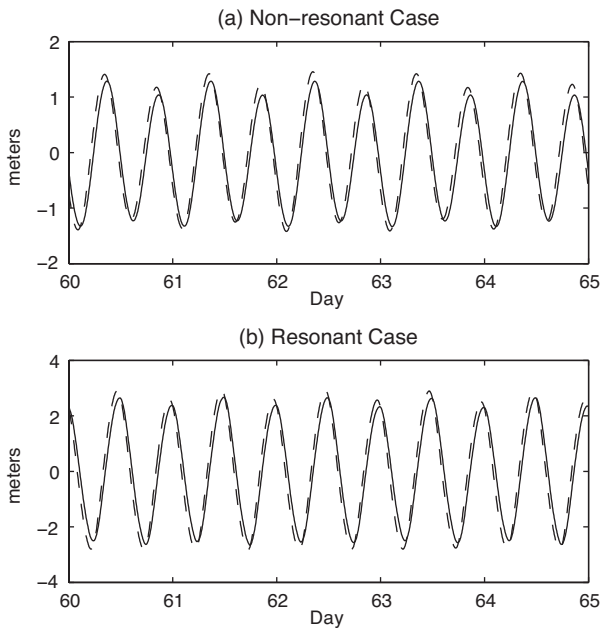


Fig. 14. Sea surface height at the head of the fjord in the full-domain (dashed line) and the Regional (solid line) models. (a) Non-resonant case. (b) Resonant case. Plotted at this scale, sea surface height in the Coastal model would be indistinguishable from that in the full-domain model.

2) *Energy Extraction Experiments*: Energy was extracted from the subdomain models in the same manner as from the full-domain model, using an enhanced drag coefficient C_E over the sill. In each case, peak extraction in a subdomain model is seen to occur at the same value of C_E as in the corresponding full domain case. The scaling relationship between the extracted energy and the tidal range reduction is

also essentially the same between the full domain and the subdomain models (Fig.15), but the maximum extracted energy is significantly different depending on the domain configuration. In the non-resonant case, the maximum extraction achieved in the Regional model is 182MW, which is 27% less than the maximum in the full-domain model; on the other hand, in the Coastal model, the maximum extractable energy is 298MW, which is 21% greater. Much of the smaller maximum extraction in the Regional model may be explained by the smaller tidal range noted in the previous section: because extraction is proportional to the cube of the current, a 9% reduction in tidal prism could account for a 27% reduction in the extraction. However, this fails to explain the larger maximum extraction achieved in the Coastal model. One possible reason for the latter is trapping of energy between the estuary and the open boundary, which due to the Dirichlet boundary conditions is reflective; a boundary condition that would allow outgoing energy to pass through may mitigate this over-estimate.

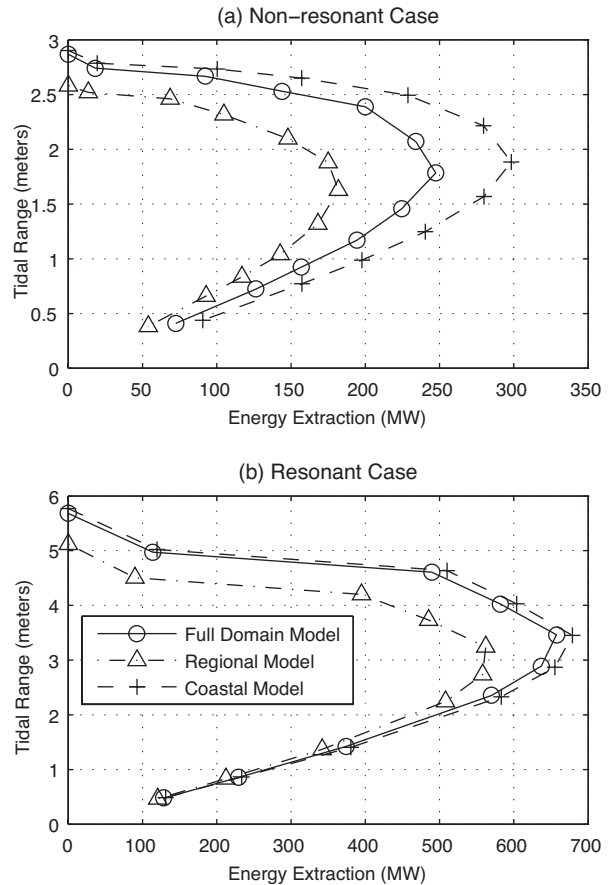


Fig. 15. Energy extraction versus tidal range for different subdomain configurations compared with the full-domain model. (a) Non-resonant case. (b) Resonant case. Legend in (b) applies to both panels.

A deficit in the maximum energy extraction in the Regional model is also seen in the resonant case (Fig.15b), with a maximum value being 562MW or 14% less than in the full-domain model. The Coastal model, on the other hand, reproduces the result of the full-domain model well: its

maximum extraction of 679MW is only 3% greater than for the full-domain model. It is also noteworthy that the larger initial “drop” in the tidal range in response to energy extraction in the resonant case is present in the subdomain models as well, indicating that this is likely a consequence of the dynamics of the resonant versus non-resonant estuary.

3) *Effect of Local Tidal Forcing*: As mentioned in Introduction, local tide-generating force is not typically included in coastal and estuarine tidal models. It is however a potential source of energy for the tides, and its absence may affect tidal energetics when energy extraction happens. In order to assess the significance of this possibility, select cases of the subdomain model runs are repeated with the tide-generating force applied.

Inclusion of local tidal forcing results in a significant improvement of tidal prediction in the Regional model. In the non-resonant case, the RMS error in sea surface height variation at the head of the fjord is reduced from 26cm to 8.6cm (from 8.5% to 2.9% of the tidal range). Other measures of the tidal performance are similarly improved. Improvements are also seen in the Coastal model, which however already performs well without local tidal forcing: the RMS error at the head of the fjord is 5.2cm without and 4.5cm with the tidal forcing.

Local tidal forcing also results in an improved prediction of maximum extractable energy in the Regional model, but the improvement is small. The maximum energy extraction is 201MW, which is 17% less than the full domain benchmark as opposed to 27% without local tidal forcing. For the Coastal model with local tidal forcing, the maximum energy extraction is 296MW, hardly changed from the case without. Thus, while applying local tide-generating force helps improve tidal prediction, its effect on the tidal energetics is less significant at least for tidal energy applications.

In the resonant case, inclusion of local tidal forcing does not significantly change subdomain model performance. The semi-diurnal amplitude in the Regional model is still deficient compared with the Full Domain model by 9.7% (as opposed to 10.8% without the local forcing); the phase discrepancy is -16.4° , in fact slightly greater than without the local forcing (-15.6°). For the Coastal model, which already performs well without tide-generating force added, the semi-diurnal discrepancy measures with the local forcing are $0.6\% / 0.8^\circ$ as opposed to $3\% / -0.05^\circ$ without, meaning that the performance of the Coastal model is good with or without local tidal forcing. Similar small effects were noted for the diurnal tide and the overall RMS error; overall, omission of local tide-generating force does not seem to amount to a critical deficiency in the tidal energetics of the models.

IV. DISCUSSION

A. Energy Extraction vs. Natural Dissipation

Perhaps the most significant result of this study concerns apportionment of energy dissipation in the estuary between naturally occurring dissipation and tidal energy extraction (Fig.11). Extraction does cause a tidal estuary to draw more

energy from the outside ocean, but this increase is less than the amount of energy extracted by the array (including “wasted” dissipation that does not result in power generation); the remainder, about half of the extracted energy at peak extraction, comes from reduction in dissipation occurring within the estuary due to natural processes. While it is somewhat misleading to think of tidal energy extraction as “diverting” energy that would be naturally dissipated, it is physically reasonable that energy extraction and consequent reduction in water movement would result in reduced dissipation elsewhere in the estuary. This finding has a couple of important implications.

First, the magnitude of naturally occurring dissipation in the estuary in an undisturbed state could influence the carrying capacity of the estuary for tidal power generation. It may be necessary to think in terms of total carrying capacity of the estuary, combining naturally occurring dissipation and man-made extraction. This means that an estimate of naturally occurring tidal dissipation would be an important part of site characterisation. On average, total energy dissipation in the estuary is balanced by influx of energy from the open ocean (Equation 7). Calculating this energy flux requires evaluation of the line integral on the right hand side of Equation (7), which in turn would require a dense sampling in space and time of current velocity and sea surface height. Alternatively, it may be diagnosed from the output of a numerical model that is well calibrated and verified (e.g. [14], [15]). However, a proxy estimate of overall energy dissipation can also be made from data on phase delays in tidal constituents spanning the length of the estuary [16], and these can be obtained from extended deployment (covering multiple spring-neap and declinational cycles) of pressure gauges throughout the estuary. Such observations would be relatively inexpensive to make, and could constitute a “second step” observational program (after a “first step” measurement of resource magnitude in terms of current strength and distribution) that would refine the assessment of tidal energy potential of an estuary. Further exploration of the significance of naturally occurring dissipation on the carrying capacity of an estuary, by varying the background drag C_N of the model within the fjord to simulate different levels of natural dissipation, is under way.

Second, tide is a source of energy for various processes that happen within an estuary, and what is represented as natural dissipation is a sum total of tidal energy going into these processes including generation of turbulence [17] and erosion, transport and deposition of sediments [18]. Less energy being available to these processes as a result of tidal energy extraction would most likely make them less active. Of particular interest is tidal generation of turbulence, which accounts for a large portion of mixing that takes place in an estuary. Reduction in tidal mixing would have a profound impact on the flushing of the estuary; because this process scales as u^3 with current speed u [19] it may be highly sensitive to energy extraction. Similarly, reduction in the energy available for resuspension and transport of sediments may cause sedimentary deposition in areas that are naturally

swept clean by the tidal current, affecting benthic habitat and perhaps even bathymetry of estuarine channels. Such environmental impacts would eventually have to be assessed with a comprehensive estuarine model that includes representation of each relevant process; however, broad-brush understanding of the magnitude of potential impacts can be gained by studying how dissipation is apportioned between natural processes and tidal energy extraction using relatively simple models such as described here.

B. Consequences of Limited Domain Representation

This study with different model configurations indicates that the character of the scaling relationship between the coefficient of energy extraction, amount of energy extraction and tidal range change is robust across a range of configurations. This indicates that the essential character of the physics of tidal energy extraction is correctly represented in a limited domain model. What does depend on the model configuration is the estimate of the maximum extractable energy. Depending on the case studied and the model configuration, this is seen to vary by as much as 27% from the “true” estimate made using the full-domain model. Since a portion of the extracted energy is sourced from the global ocean beyond the subdomain model boundary, and since the boundary condition for the subdomain model is not guaranteed to adapt to the changed energy flux (with Dirichlet boundary conditions, the energy flux at the boundary is fixed), it is perhaps not surprising that limited domain representation introduces quantitative uncertainty into resource assessment.

While only a couple of domain configurations were tried here, their results indicate that the error in the extraction limit estimate may not scale simply with the domain size. The larger of the two subdomain models (the “Regional”) underestimates the extraction limit, while the smaller (the “Coastal”) gives an overestimate. Further experiments with different domain configurations may lead to a more refined understanding of how they affect the estimate, and may lead to an implementation guideline for a regional model towards minimizing the error. Experiments with alternative boundary conditions ([20], [21]) and exploration of mitigating measures [6] would be worth undertaking and are planned for the future. However, given the complexity of the pattern of energy flux change that occurs as a result of energy extraction (Fig.13), it may not be possible to come up with a simple set of rules for an optimal placement of model boundaries. Also, in reality, where to place the model boundary may be determined by where data that can be used for boundary conditions is available, and thus there may not be much flexibility in its choice. At this point at least, limited domain representation needs be considered a source of uncertainty in the estimate of maximum extractable tidal energy. From this study, the level of this uncertainty appears to be of the order of $\pm 25\%$. This may be an acceptable level of uncertainty for an initial, screening-level resource assessment to determine whether or not a particular site warrants further consideration. Once it is determined that a site is worth developing, efforts should go into development of a detailed hydrodynamic model for the region including the site and into data collection for model

verification and pre/post development monitoring. An adaptive management framework, where monitoring data and model results are incorporated into an ever more refined estimate of the impact scaling as the site is developed, may also give us the eventual extraction limit.

C. Scaling at Low Levels of Extraction

One result of this model study that requires a remark is what appears to be a distinct scaling regime between energy extraction and tidal range change (equivalent to the change in tidal prism) at the lowest levels of extraction (Figs.8c and 15). Tidal range seems relatively sensitive to energy extraction in this regime, while at higher levels of extraction more energy can be harvested with relatively less change in the tidal range, before the physical extraction limit is approached. This regime appears in all cases studied here, including the resonant and non-resonant cases and the full-domain and the subdomain models. As far as we are aware of, this regime has not been previously reported; however, it is still possible that this is specific to the particular estuary configuration used in this study, or even a numerical artifact specific to the model code. At this stage, caution must be exercised against attaching significance to this finding. Further investigation of the robustness of this regime using multiple alternative models is planned. If this regime is real, it will have implications on adaptive management strategy for tidal energy development: directly extrapolating maximum energy extraction (whether physical or in terms of environmental impact limit) from an initially observed scaling as tidal power array is developed may give too pessimistic an estimate of the overall potential.

ACKNOWLEDGMENT

Material presented in this paper is based upon work supported by the U.S. Department of Energy under Award Number DE-FG36-08GO18179. During preparation of this paper, the first author was also supported by National Science Foundation grant CHE-1230426. The authors thank Dr. Brian Polagye for encouragement and stimulating discussions, and for his leadership in moving marine renewable energy research forward.

Disclaimer. This report was prepared as an account of work sponsored by an agency of the United States Government. Neither the United States Government nor any agency thereof, nor any of their employees, makes any warranty, expressed or implied, or assumes any legal liability or responsibility for the accuracy, completeness, or usefulness of any information, apparatus, product, or process disclosed, or represents that its use would not infringe privately owned rights. Reference herein to any specific commercial product, process, or service by trade name, trademark, manufacturer, or otherwise does not necessarily constitute or imply its endorsement, recommendation, or favoring by the United States Government or any agency thereof. Their views and opinions of the authors expressed herein do not necessarily state or reflect those of the United States Government or any agency thereof.

REFERENCES

- [1] R. H. Karsten, J. M. McMillian, M. J. Lickley, and R. D. Haynes, "Assessment of tidal current energy in Minas Passage, Bay of Fundy," *Proc. IMechE, Part A: J. Power Energy*, vol. 222, pp. 493–507, Aug. 2008.
- [2] D. Hasegawa, J. Sheng, D. A. Greenberg, and K. R. Thompson, "Far-field effects of tidal energy extraction in the Minas Passage on tidal circulation in the Bay of Fundy and Gulf of Maine using a nested-grid coastal circulation model," *Ocean Dynamics*, vol. 61, pp. 1845–1868, Nov. 2011.
- [3] N. Yates, I. Walkington, R. Burrows, and J. Wolf, "Appraising the extractable tidal energy resource of the UK's western coastal waters," *Phil. Trans. R. Soc. A*, 371, 20120181, Jan. 2013.
- [4] D. T. Pugh, *Changing Sea Levels: Effects of Tides, Weather and Climate*, Cambridge, United Kingdom: Cambridge University Press, 2004.
- [5] C. Garrett, and D. Greenberg, "Predicting changes in tidal regime: the open boundary problem," *J. Phys. Oceanogr.*, vol. 7, pp. 171–181, Mar. 1977.
- [6] T. A. A. Adcock, A. G. L. Borthwick, and G.T. Houlby, "The open boundary problem in tidal basin modelling with energy extraction," in *Proc. 9th European Wave and Tidal Energy Conference*, Sep. 2011.
- [7] C. Garrett and P. Cummins, "The power potential of tidal currents in channels," *Proc. R. Soc. Lond. A*, vol. 461, pp. 2563–2572, Aug. 2005.
- [8] I. G. Bryden and S. J. Couch, "How much energy can be extracted from moving water with a free surface: A question of importance in the field of tidal current energy?," *Renewable Energy*, vol. 32, pp. 1961–1966, Sep. 2007.
- [9] A. E. Gill, *Atmosphere-Ocean Dynamics*, London, United Kingdom: Academic Press, 1982.
- [10] D. B. Haidvogel, H. Arango, W. P. Budgell, B. D. Cornuelle, E. Curchitser, E. Di Lorenzo, K. Fennel, W. R. Geyer, A. J. Hermann, L. Lanerolle, J. Levin, J. C. McWilliams, A. J. Miller, A. M. Moore, T. M. Powell, A. F. Shchepetkin, C. R. Sherwood, R. P. Signell, J. C. Warner, and J. Wilkin, "Ocean forecasting in terrain-following coordinates: Formulation and skill assessment of the Regional Ocean Modeling System," *J. Comput. Phys.*, vol. 227, pp. 3595–3624, Mar. 2008.
- [11] W. Munk and C. Wunsch, "Abyssal recipes II: energetics of tidal and wind mixing," *Deep-Sea Res. I*, vol. 45, pp. 1977–2010, Dec. 1998.
- [12] J. Blanchfield, C. Garrett, P. Wild, and A. Rowe, "The extractable power from a channel linking a bay to the open ocean," *Proc. IMechE, Part A: J. Power Energy*, vol. 222, pp. 289–297, May 2008.
- [13] B. Polagye, P. Malte, M. Kawase, and D. Durran, "Effect of large-scale kinetic power extraction on time-dependent estuaries," *Proc. IMechE, Part A: J. Power Energy*, vol. 222, pp. 471–484, Aug. 2008.
- [14] B. Polagye, M. Kawase, and P. Malte, "In-stream tidal energy potential of Puget Sound, Washington," *Proc. IMechE, Part A: J. Power Energy*, vol. 223, pp. 571–587, Aug. 2009.
- [15] M. C. Easton, D. K. Woolf, and P. A. Bowyer, "The dynamics of an energetic tidal channel, the Pentland Firth, Scotland," *Continental Shelf Res.*, vol. 48, pp. 50–60, Oct. 2012.
- [16] H. J. Freeland and D. M. Farmer, "Circulation and energetics of a deep, strongly stratified inlet," *Can. J. Fish. Aquat. Sci.*, vol. 37, pp. 1398–1410, Sep. 1980.
- [17] G. Abraham, "Turbulence and mixing in stratified tidal flows," in *Physical Processes in Estuaries*, J. Dronkers and W. van Leussen, Eds., Berlin, Germany: Springer-Verlag, 1988, pp. 149–180.
- [18] H. Postma, "Sediment transport and sedimentation in the estuarine environment," in *Estuaries, American Association for the Advancement of Science Publication*, 83, G. H. Lauff, Ed., 1967, pp. 158–179.
- [19] J. H. Simpson and D. Bowers, "Models of stratification and frontal movement in shelf seas," *Deep-Sea Res.*, vol. 28A, pp. 727–728, Jul. 1981.
- [20] R. A. Flather, "A tidal model of the northwest European continental shelf," *Mem. Soc. R. Sci. Liege*, vol. 10, pp. 141–164, 1976.
- [21] D. C. Chapman, "Numerical treatment of cross-shelf open boundaries in a barotropic coastal ocean model," *J. Phys. Oceanogr.*, vol. 15, pp. 1060–1075, Aug. 1985.